Journal of Alloys and Compounds 509 (2011) 7625–7631

Contents lists available at ScienceDirect

Journal of Alloys and Compounds

journal homepage: www.elsevier.com/locate/jallcom

Structural, absorption and fluorescence spectral analysis of Pr^{3+} ions doped zinc bismuth borate glasses

Inder Pal [a], Ashish Agarwal [a,*], Sujata Sanghi [a], M.P. Aggarwal [b]

[a] Department of Applied Physics, Guru Jambheshwar University of Science and Technology, Hisar 125001, Haryana, India
[b] Department of Physics, Guru Nanak Khalsa College, Yamunanagar 135001, Haryana, India

ARTICLE INFO

Article history:
Received 23 January 2011
Received in revised form 19 April 2011
Accepted 21 April 2011
Available online 28 April 2011

Keywords:
Judd–Ofelt parameters
Radiative life-time
Branching ratio
Stimulated emission cross section
Pr^{3+} doped glasses

ABSTRACT

Glasses having composition $20ZnO{\cdot}xBi_2O_3{\cdot}(79.5-x)B_2O_3{\cdot}0.5Pr_6O_{11}$ were prepared by melt quench technique. The amorphous nature of the prepared glass samples was confirmed by X-ray diffraction. The spectroscopic properties of these glasses were investigated by recording optical absorption and fluorescence spectra. The structural investigations of the glasses were carried out by recording the IR spectra. The optical properties of Pr^{3+} ions doped zinc borate glasses with varying concentration of bismuth oxide have been studied. The Judd–Ofelt intensity parameters Ω_λ ($\lambda = 2, 4, 6$) and other radiative properties like radiative transition probability, radiative life time, branching ratio and stimulated emission cross-section of the prepared glasses have been calculated. The variation of Ω_2 with Bi_2O_3 content has been attributed to changes in the asymmetry of the ligand field at the rare earth ion site and to the changes in their rare earth oxygen (*RE-O*) covalency. The branching ratio for $^3P_0 \rightarrow {}^3F_2$ transition is 42% and the predicted spontaneous radiative transition probability rates are fairly high (14,347–14,607 s^{-1}). This is beneficial for lasing emission. The stimulated emission cross-section for all the emission bands has been calculated.

1. Introduction

Rare-earth (*RE*) doped glasses play a very significant role in the development of lasers and fibre amplifiers for optical telecommunication. The optical properties of *RE* ions are slightly influenced by the ligand field surrounding them. Among the rare earth ions, trivalent praseodymium ions (Pr^{3+}) have different applications due to a large number of available absorption bands in the *UV*, visible and near infrared regions. It is used for optical amplifiers, up-converters and other electro optic devices [1–3]. Spectral properties of Pr^{3+} ions doped glasses have been widely investigated because the energy levels of Pr^{3+} ions are such that the emission spectrum ranges from UV to infrared. Pr^{3+} ions doped glass fibre are currently used as promising device for optical communication system based on 1.3 μm radiation [4]. Laser action has been observed for $^1D_2 \rightarrow {}^3H_4$ transition [5–7] of the Pr^{3+} ions. Pr^{3+} ions doped alkali bismuth gallate [8], TeO_2–LiF [9], lithium borate, lithium fluoro-borate [10] and oxyfluoro-borate [11] glasses have been studied. Pr^{3+} doped heavy metal oxide glasses such as germanate, lead oxide, bismuth oxide and tellurite glasses have proved to be effective for several practical applications [12] because of their high refractive index, high transmittance for infrared radiation and high chemical stability. Tellurite and heavy metal oxide glasses have been paid much attention in recent years because their maximum phonon energy is lower in comparison to borate, phosphate and silicate glasses. The emission quantum efficiency from a given level strongly depends on the phonon energy of the host medium. It is expected that the non-radiative losses to the lattice will be small and the fluorescence quantum efficiency will be high in tellurite and heavy metal oxide glasses [13,14]. The intensity of the transitions for the rare earth ions has been calculated by using the Judd–Ofelt theory [15,16]. This theory defines a set of three intensity parameters Ω_λ ($\lambda = 2, 4, 6$) which are sensitive to the environment of the rare earth ions. These intensity parameters have been used to calculate important optical properties such as radiative transition probability for spontaneous emission, radiative life time of the excited state, branching ratio and stimulated emission cross-section in order to optimize the best configuration of the ion- host to improve the laser efficiency of a specific electronic transition. The intensity parameter Ω_2 is an indicator of the covalency of the rare earth-oxygen bond and it is sensitive to the structural changes in the glass. In bismuth borate glasses, Ω_2 varies due to the conversion of three coordinated boron atoms (B_3) to four coordinated boron atoms (B_4) and the change in the number of non-bridging oxygens ions (NBO's).

In this paper, we have studied the effect of bismuth oxide on the absorption and emission properties of Pr^{3+} doped zinc bismuth borate glasses. We have chosen this heavy metal based glasses to

* Corresponding author. Tel.: +91 1662 263384; fax: +91 1662 276240.
E-mail address: aagju@yahoo.com (A. Agarwal).

0925-8388/$ – see front matter © 2011 Elsevier B.V. All rights reserved.
doi:10.1016/j.jallcom.2011.04.114

incorporate the Pr^{3+} ions because these glasses have large glass forming region, high refractive index, good physical and chemical stability and large transmission window.

2. Judd–Ofelt theory

The absorption spectra of rare earth ions serve as a basis for understanding their radiative properties. The sharp absorption lines arising from the 4*f*–4*f* electronic transitions can be electric dipole, magnetic dipole or electric quadrupole in character. The quantitative calculation of the intensities of these transitions has been developed independently by Judd [15] and Ofelt [16]. A brief outline of the Judd–Ofelt theory is given below:

For a rare earth ion, the electric dipole transitions between two states within the 4*f* configuration are parity forbidden, while the magnetic dipole and electric quadrupole transitions are allowed. For an ion in a medium, the electric dipole transitions become allowed due to the admixture of states from configuration of opposite parity (for example $4f^{N-1}\ 5d$) into the 4*f* configuration. The transition probability depends on the extent of admixture. The intensity of an absorption band is expressed in terms of a quantity called the "oscillator strength". Experimentally, it is given by the area under the absorption band and can be expressed in terms of the absorption coefficient, $\alpha(\lambda)$ at a particular wavelength λ and is given by [17]:

$$f_{\text{expt}} = \frac{mc^2}{\pi e^2 N}\int \frac{\alpha(\lambda)d\lambda}{\lambda^2} \tag{1}$$

where $\alpha(\lambda) = (2.303)OD(\lambda)/d$ $OD(\lambda)$ is the optical density, d is the thickness of the sample, *m* and *e* are the mass and charge of electron, respectively, *c* is the velocity of light and *N* is the number of rare earth ions per unit volume.

According to the Judd–Ofelt theory [18], the oscillator strength of a transition between an initial *J* manifold (*S*,*L*) *J* and a final *J*′ manifold (*S*′,*L*′)*J*′ is given by:

$$f_{cal}(aJ, bJ') = \frac{8\pi^2 m\nu}{3h(2J+1)}\left[\frac{(n^2+2)^2}{9n}S_{ed} + nS_{md}\right] \tag{2}$$

where

$$S_{ed}\left[(S,L)J,(S',L')J'\right] = \sum_{\lambda=2,4,6}\Omega_\lambda\left|\left\langle (S,L)J\left\|U^{(\lambda)}\right\|(S',L')J'\right\rangle\right|^2$$

and

$$S_{md}\left[(S,L)J,(S',L')J'\right] = \sum_{\lambda=2,4,6}\Omega_\lambda\left|\left\langle (S,L)J\left\|L+2S\right\|(S',L')J'\right\rangle\right|^2$$

S_{ed} and S_{md} represent the line strengths for the induced electric dipole transitions and the magnetic dipole transitions, respectively.

The three intensity parameters, Ω_λ ($\lambda = 2, 4, 6$) are characteristic of a given rare earth ion (in a given matrix) and are related to the radial functions of the states $4f^N$, the admixing states $4f^{N-1}5d$ or $4f^{N-1}5g$ and the ligand field parameters that characterize the environmental field. These are given by the expression:

$$\Omega_\lambda = (2\lambda+1)\sum_{s,p}\left|A_{s,p}\right|^2\Xi^2(s,\lambda)(2S+1)^2,\ \lambda = 2,4,6 \tag{3}$$

where $A_{s,p}$ are the crystal field parameters of rank *s* and are related to the structure around the rare earth ion. $\Xi(s,\lambda)$ is related to the matrix elements between the radial wave functions of 4*f* and admixing levels, e.g., 5*d*, 5*g* and the energy difference between two levels. $\left|\left\langle\left\|U^{(\lambda)}\right\|\right\rangle\right|^2$ represents the square matrix elements of the unit tensor operators $U^{(\lambda)}$ connecting the initial and final states. The matrix elements are calculated in the intermediate coupling approximation [19]. Due to the electrostatic shielding of the 4*f* electrons by the closed 5*p* shell electrons, the matrix elements of the unit tensor operator between two energy manifolds in a given rare earth ion do not vary significantly when it is incorporated in different hosts. Therefore, the matrix elements computed for the free ion may be used for calculation in different media and are reported by Weber et al. [20] and Carnall et al. [21]. The reduced matrix elements $\left\langle\left\|L+2S\right\|\right\rangle$ for magnetic dipole transitions are reported by Neilson et al. [22].

The values of Ω_λ obtained from the absorption measurements are used to calculate the radiative transition probability, radiative lifetime of the excited states, branching ratio (which predict the fluorescence intensity of the lasing transition) and stimulated emission cross-section. The radiative transition probability A_{rad} (*aJ*, *bJ*′) for emission from an initial state *aJ* to a final *bJ*′ is given by [23]:

$$A_{rad}(aJ, bJ') = \frac{64\pi^4\nu^3e^2}{3hc^3(2J+1)}\left[\frac{n(n^2+2)^2}{9}S_{ed} + n^3S_{md}\right] \tag{4}$$

In case of electric dipole emission, this equation becomes:

$$A_{rad}(aJ, bJ') = \frac{64\pi^4\nu^3e^2}{3hc^3(2J+1)}\frac{n(n^2+2)^2}{9} \times \sum_{\lambda=2,4,6}\Omega_\lambda\left|\left\langle (S,L)J\left\|U^{(\lambda)}\right\|(S',L')J'\right\rangle\right|^2 \tag{5}$$

The total radiative emission probability, $A_T(aJ)$ of the excited state *SLJ* is given by the sum of the A_{rad} (*aJ*,*bJ*′) terms calculated over all terminal states *b*:

$$A_T(aJ) = \sum_{bJ'}A_{rad}(aJ, bJ') \tag{6}$$

The fluorescence branching ratio β_r is given as:

$$\beta_r = \frac{A_{rad}(aJ, bJ')}{A_T(aJ)} \tag{7}$$

The radiative lifetimes of the emission state is:

$$\tau_r = \frac{1}{A_T(aJ)} \tag{8}$$

Finally, the stimulated emission cross-section of the fluorescent level is given by:

$$\sigma = \frac{\lambda_p^4 A_{rad}(aJ, bJ')}{8\pi cn^2\Delta\lambda} \tag{9}$$

3. Experimental details

The Pr^{3+} ions doped glasses having composition $20ZnO{\cdot}xBi_2O_3{\cdot}(79.5-x)B_2O_3{\cdot}0.5Pr_2O_{11}$ ($15 \le x \le 35$ *x* in mol%) were prepared by using melt-quenching technique. The 15*g* batches of analar grade chemicals were taken in appropriate proportion and were melted at 1150 °C for 40 min. The melt was stirred frequently for homogeneous mixing of all the constituents. The glass samples were obtained by pouring and quenching the melt in between two stainless steel plates held at room temperature (*RT*). The amorphous nature of the prepared samples was confirmed by recording X-ray diffraction patterns using Miniflex-II (Rigaku) X-ray diffractometer. The density (*D*) of each glass sample was measured by the Archimedes's principle using Xylene as immersing liquid. The refractive index (*n*) of the polished samples was measured by the Brewster angle method using He–Ne laser (632 nm). The optical absorption spectra of all the polished samples were recorded at RT in the wavelength range 300–3200 nm using a spectrophotometer (Varian-Carry 5000). The emission spectra were recorded using a spectroflurometer (JobinYvon Fluorolog-3) at an excitation wavelength of 450 nm.

The IR spectra of all the samples were recorded in the range 400–4000 cm^{-1} at RT with a spectral resolution of 4 cm^{-1} using FTIR spectrometer (Shimadzu FTIR 8001PC).

Table 1
Density (D), molar volume (V_M), no. density of Pr^{3+} ions (N), refractive index (n), dielectric constant (ε), reflection loss (R_L), inter-ionic distance (r_i) and ionic radius (r_p) for $20ZnO{\cdot}xBi_2O_3$ $(79.5-x)B_2O_3{\cdot}0.5Pr_6O_{11}$ glasses.

Sample code	x (mol%)	D (g/cm^3)	V_M (cm^3/mol)	N (10^{20} ions/cm^3)	n	ε (n^2)	R_L(%) $[(n-1)/(n+1)]^2$	r_i (Å)	r_p (Å)
ZBP1	15	4.41	29.79	7.01	1.75	3.06	7.44	2.43	0.97
ZBP2	20	4.72	32.06	6.83	1.80	3.24	8.16	2.45	0.98
ZBP3	25	5.06	33.92	6.70	1.86	3.46	9.04	2.46	0.99
ZBP4	30	5.27	36.42	6.44	1.89	3.57	9.48	2.49	1.01
ZBP5	35	5.55	38.18	6.30	1.94	3.76	10.52	2.51	1.09

4. Results and discussion

4.1. Absorption spectra and oscillator strength

The X-ray diffraction patterns of all the glasses are shown in Fig. 1 and the amorphous nature of the prepared samples is confirmed. From the measured values of density (D), molar volume (V_M) and refractive index (n), various other physical parameters such as Pr^{3+} ion concentration (N), dielectric constant (ε), reflection loss (R_L), mean rare earth ion separation (r_i) and ionic radius (r_p) of these glasses are evaluated using the conventional formulae and are presented in Table 1.

The optical absorption spectra of ZBP1 glass sample are shown in Fig. 2. From these spectra, absorption bands at 444, 468, 482, 588, 904, 1422, 1520, and 1884 nm are observed and these bands are assigned to following transitions for Pr^{3+} ion: $^3H_4 \rightarrow {}^3P_{2,1,0}$, $^3H_4 \rightarrow {}^1D_2$, $^3H_4 \rightarrow {}^1G_4$, and $^3H_4 \rightarrow {}^3F_{4,3,2}$, respectively. These bands correspond to the $4f^2$-configuration electric dipole transitions from the ground state ($^3H_4$) to the various excited states and the band width are due to the combination of inhomogeneous broadening and unresolved stark splitting. The observed absorption bands can be divided into three groups; transition from $^3H_4 \rightarrow {}^1G_4$ and $^3H_4 \rightarrow {}^3F_{4,3,2}$ in the infrared region, the $^3H_4 \rightarrow {}^1D_2$ transition at 588 nm and $^3H_4 \rightarrow {}^3P_{2,1,0}$, complex group of transitions in violet to blue region. For calculating oscillator strength of the overlapped peaks, the area of the peaks was estimated by extrapolating up to the base line. In order to estimate the intensities for the transitions $^3H_4 \rightarrow {}^3P_{2,1,0}$, it is first noted that the base line for the absorption is rising towards the higher frequency side. Since the peaks are distinct we extended the two sides of individual lines linearly to this base line and measured each such triangular area. In the region of overlap, the proportion of intensity contributed by different transitions is so adjusted that the relative intensities as estimated by the peak height are not unduly modified. The experimental oscillator strengths, which measure the intensity of absorption transitions from the ground $^3H_4$ level to various excited levels, have been measured by Eq. (1) and the values are given in Table 2. The transitions $^3H_4 \rightarrow {}^3P_2$ and $^3H_4 \rightarrow {}^3F_2$ of Pr^{3+} ions have been labeled as hypersensitive transitions as these transitions are strongly dependent on the neighbouring ligands [24] and these obey the selection rules: $\Delta S = 0$, $\Delta L \leq 2$ and $\Delta J \leq 2$ [25].

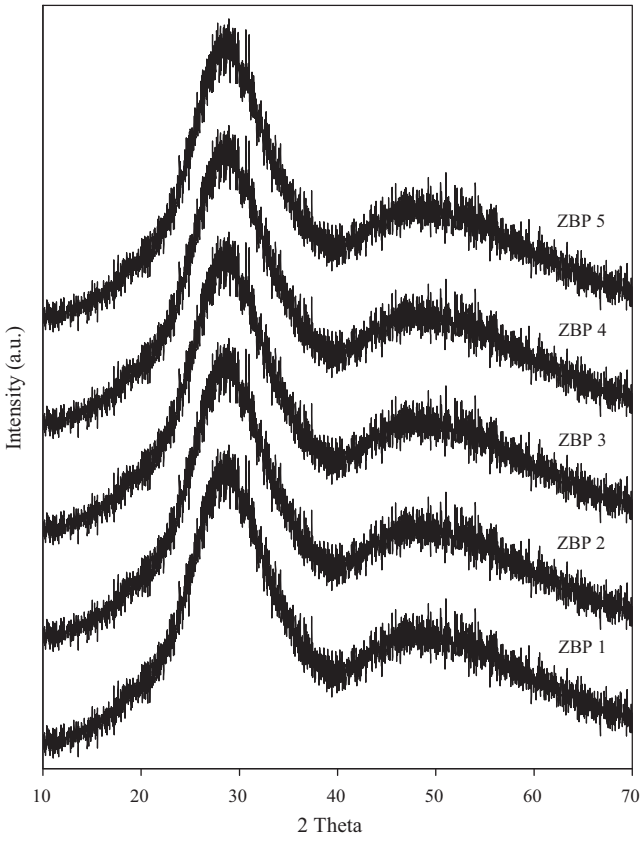

Fig. 1. XRD patterns of $20ZnO{\cdot}xBi_2O_3{\cdot}(79.5-x)B_2O_3{\cdot}0.5Pr_6O_{11}$ (ZBP) glasses.

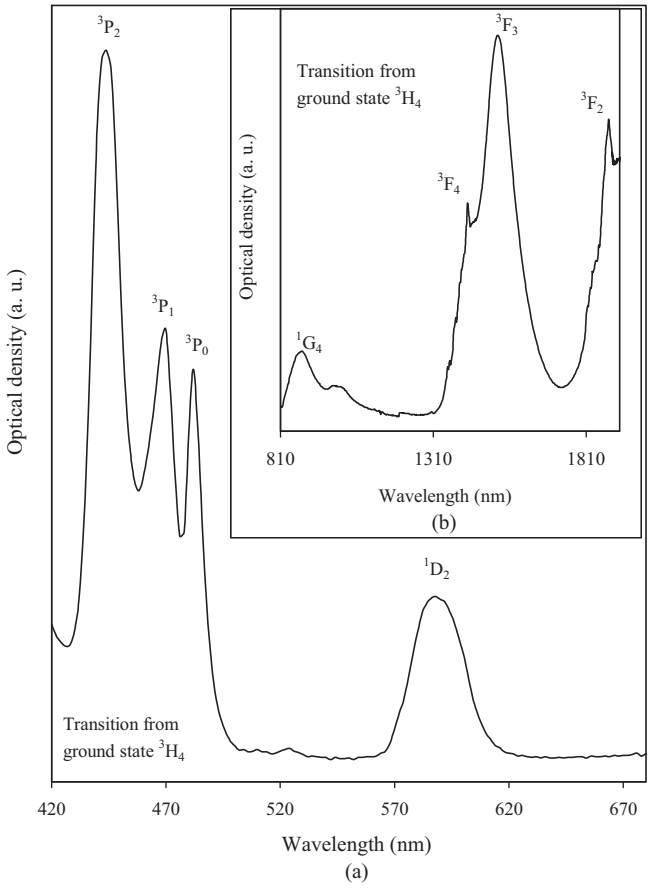

Fig. 2. Optical absorption spectra of ZBP1 glass sample in. (a) The visible region (b) near IR region.

Table 2
Oscillator strength for some transitions from the indicated levels to the ground level $^3H_4$, and their root mean square (δ_{RMS}), which indicates the fit quality of theoretical and experimental results for $20ZnO{\cdot}xBi_2O_3{\cdot}(79.5-x)B_2O_3{\cdot}0.5Pr_6O_{11}$ glasses.

Transitions from ground level	λ(nm)	Oscillator strength (10^{-6})									
		ZBP1		ZBP2		ZBP3		ZBP4		ZBP5	
$^3H_4\rightarrow$		f_{expt}	f_{cal}	f_{expt}	f_{cal}	f_{expt}	f_{cal}	f_{expt}	f_{cal}	f_{expt}	f_{cal}
$^3P_2$	422	4.90	5.09	3.29	4.69	3.09	4.26	2.89	3.79	2.17	2.31
$^3P1$	468	2.83	2.34	1.81	1.68	1.71	1.57	1.59	1.51	1.04	1.11
$^3P0$	482	1.98	2.31	1.42	1.66	1.37	1.55	1.29	1.48	0.99	1.10
$^1D_2$	588	0.99	1.42	0.78	1.01	0.69	1.25	0.56	1.11	0.38	0.67
$^1G_4$	916	0.71	0.63	0.64	0.57	0.58	0.41	0.49	0.34	0.27	0.32
$^3F_4$	1422	6.21	5.29	5.26	4.97	4.89	4.48	4.07	3.97	3.47	3.49
$^3F_3$	1520	8.38	8.24	8.08	7.53	7.42	6.82	6.74	6.09	6.18	5.26
$^3F_2$	1884	1.57	1.63	1.75	1.88	1.59	1.69	1.38	1.47	1.09	1.22
$\delta_{RMS}(10^{-7})$			7.34		8.08		6.80		5.71		7.11

The oscillator strength of these peaks shows a peculiar behavior, the strength decreases as Bi_2O_3 concentration increases from 15 to 35 mol%, the data are given in Table 2. Using the experimental oscillator strengths, the host dependent Judd–Ofelt intensity parameters Ω_λ ($\lambda = 2,4,6$) and calculated oscillator strength for observed electric dipole transitions within the $4f^2$ configuration have been determined using the Eq. (2) by least square fit procedure (Table 2).

The reduced matrix elements $\left\|U^{(\lambda)}\right\|^2$ that are insensitive to the environment of rare earth ions were taken from the literature [21]. An immediate measure of the quality of the fit is given by the root mean square deviation (δ_{RMS}) between the experimental and calculated oscillator strength and is represented by:

$$\delta_{RMS} = \left[\frac{\sum (f_{exp\ \ t} - f_{cal})^2}{P}\right]^{1/2} \quad (10)$$

where P is the total number of energy levels included in the fitting procedure.

It has been noted that the Judd–Ofelt theory is not very successful in case of Pr^{3+} ion as the energy levels corresponding to the ground configuration $4f^2$ and the first excited $4f^15d^1$ state differ very little in energy [26]. Because of this small energy separation, a negative value for the parameter Ω_2 has been reported [27] and there is usually a poor agreement between the theoretically estimated and experimentally measured results for various optical parameters [27]. Many authors [28–30] have therefore excluded the $^3H_4 \rightarrow {}^3P_2$ transition in applying the Judd–Ofelt theory to the observed spectrum of Pr^{3+} ions. The Judd–Ofelt parameters have been recalculated after excluding this transition but it was noted that neither the calculated oscillator strength nor the δ_{RMS} deviation showed any significant improvement. Therefore, in the present work the Judd–Ofelt parameters have been calculated by including $^3H_4 \rightarrow {}^3P_2$ transition. Further, no unphysical (like negative) values for Ω_2 have been found but the agreement with experimental results is not good for $^3H_4 \rightarrow {}^3P_2$ transition. For other transitions, including the second hypersensitive transition ($^3H_4 \rightarrow {}^3F_2$), the agreement is reasonably good. The values of Judd–Ofelt intensity parameters are given in Table 3 along with the values of some other glasses for comparison. Table 3 shows that Ω_2 increases whereas Ω_4 and Ω_6 decrease with increase in the Bi_2O_3 content in the host glasses. These intensity parameters reflect the local structure and bonding in the vicinity of rare earth ions to some extent. As a general conclusion, Ω_2 parameter increases with asymmetry of the local structure and with the degree of covalency of the lanthanide-ligand bonds, whereas Ω_6 parameter decreases with the tendency of covalency. In addition, Ω_4 parameter is believed to be related to the bulk properties of the samples [31]. Ω_2 is higher for the present glasses in comparison to oxy-fluoride [31], tellufluoro-phosphate [32], fluorozirconate [33], mixed-halide [33] and ZBLAN glasses [34] except for ZBP 1 glass sample. This indicates that the asymmetry and covalency of Pr^{3+} ions in the zinc bismuth borate glasses are stronger than those in the others glasses mentioned above. The lower value of Ω_2 for ZBP1 glass indicates that for smaller concentration of Bi_2O_3 (15 mol%), the asymmetry of the ligand field is minimum. It has been reported in Sm^{3+} ions doped zinc bismuth borate glasses [35] that the addition of Bi_2O_3 in the glass converts BO_3 units into BO_4 units. An increased formation of BO_4 units leads to close packing of oxygen atoms around the rare earth ion resulting in higher symmetry around the rare earth site. Also the intensity parameters, Ω_λ ($\lambda = 2, 4, 6$) and the spectroscopic quality factor (SQF) (Table 3) as well as the radiative properties like radiative transition probability (A_{rad}), radiative lifetime of the excited states (τ_r), branching ratio (β_r) and stimulated emission cross-section (σ) (Table 4) obtained in the present ZBP glasses follow the same trend as predicted in the Sm^{3+} ions doped zinc bismuth borate glasses [35].

Table 3
Judd–Ofelt intensity parameters (Ω_2, Ω_4, Ω_6) of Pr^{3+} ions doped glasses.

Glass	Ω_2 (10^{-20} cm^2)	Ω_4 (10^{-20} cm^2)	Ω_6 (10^{-20} cm^2)	SQF (Ω_4/Ω_6)	References
ZBP1	1.30	3.29	2.13	1.54	Present work
ZBP2	2.69	2.27	2.03	1.12	Present work
ZBP3	2.89	2.04	1.99	1.03	Present work
ZBP4	3.27	1.88	1.32	1.42	Present work
ZBP5	3.94	1.34	1.23	1.09	Present work
Oxyfluoride	0.13	4.09	6.33	0.65	[31]
LiTFP	0.264	8.067	5.884	1.37	[32]
NaTFP	0.229	7.312	6.149	1.19	[32]
KTFP	0.498	8.814	6.426	1.37	[32]
Fluorozirconate	2.8	4.9	5.3	0.92	[33]
Mix-Halide	2.7	4.4	5.4	0.81	[33]
ZBLAN	2.44	4.41	5.52	0.79	[34]

Table 4
The peak wavelength (λ_p), radiative transition probability (A_{rad}), branching ratio (β_r), stimulated emission cross-section (σ), total radiative transition probability (A_T), radiative life time (τ_r) and the total emission cross-section (σ_t) for various transitions in $20ZnO.xBi_2O_3$ $(79.5-x)B_2O_3.0.5Pr_6O_{11}$ glasses.

Transitions	ZBP1				ZBP2			ZBP3			ZBP4			ZBP5		
	λ_p (nm)	A_{rad} (s^{-1})	β_r (%)	σ (10^{-20} cm^2)	A_{rad} (s^{-1})	β_r (%)	σ (10^{-20} cm^2)	A_{rad} (s^{-1})	β_r (%)	σ (10^{-20} cm^2)	A_{rad} (s^{-1})	β_r (%)	σ (10^{-20} cm^2)	A_{rad} (s^{-1})	β_r (%)	σ (10^{-20} cm^2)
$^3P_0 \rightarrow {}^3H_4$	493	11,020	0.325	4.03	11,080	0.325	4.48	11,189	0.324	5.07	11,269	0.325	6.51	11,286	0.323	7.13
$^3P_0 \rightarrow {}^3H_6$	608	6931	0.205	1.58	6980	0.205	1.69	7003	0.202	1.73	7098	0.204	1.89	7130	0.204	2.20
$^3P_0 \rightarrow {}^3F_2$	644	14,347	0.423	13.36	14,400	0.422	14.91	14,584	0.422	16.83	14,505	0.417	18.65	14,607	0.418	18.86
$^3P_0 \rightarrow {}^3F_3$	723	956	0.028	1.62	976	0.029	1.67	1037	0.030	2.75	1099	0.032	2.81	1112	0.032	3.20
$^1D_2 \rightarrow {}^3H_6$	787	633	0.019	1.17	656	0.019	1.85	719	0.021	2.50	748	0.022	2.72	795	0.023	2.94
$A_T(s^{-1})$		33,887			34,092			34,532			43,719			34,930		
$\tau_r(\mu s)$		29.51			29.33			28.96			28.80			28.63		
$\sigma_t(10^{-20}$ $cm^2)$		21.76			24.60			28.88			32.58			34.33		

Fig. 3. Fluorescence spectra of ZBP1 and ZBP 5 glass samples.

4.2. Fluorescence spectra

Fig. 3 shows the fluorescence spectra for ZBP1 and ZBP5 glass samples recorded at RT (λ_{ext} = 450 nm). This figure shows five peaks around 493, 608, 644, 724, and 787 nm. These fluorescence peaks are assigned to $^3P_0 \rightarrow {}^3H_{4,6,}$ $^3P_0 \rightarrow {}^3F_{2,3}$ and $^1D_2 \rightarrow {}^3H_6$ transitions, respectively. The assignment of the peaks to specific transitions have been made on the basis of known energy levels of Pr^{3+} ions as reported by Dieke [36] and earlier workers [10,11]. The first and most interesting observation is that the intensity of the fluorescence peak at 493 nm corresponding to $^3P_0 \rightarrow {}^3H_4$ transition increases with increasing Bi_2O_3 concentration. The another important observation is that the last two peaks $^3P_0 \rightarrow {}^3F_3$ and $^1D_2 \rightarrow {}^3H_6$ have very low intensity for ZBP1 glass and the intensity for these transitions increases with increasing Bi_2O_3 which may be attributed to the structural change.

Fig. 4. Energy levels depicting the various lasing transitions of Pr^{3+} ions. ($^3P_0 \rightarrow {}^3H_{4,6,}$ $^3P_0 \rightarrow {}^3F_{2,3}$ and $^1D_2 \rightarrow {}^3H_6$)

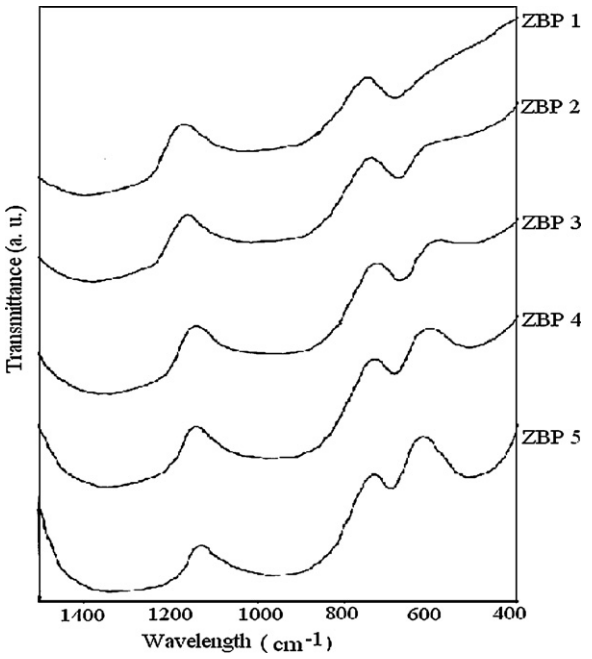

Fig. 5. Infrared transmission spectra of $20ZnO{\cdot}xBi_2O_3{\cdot}(79.5-x)B_2O_3{\cdot}0.5Pr_6O_{11}$ glasses.

The fluorescence spectra have been used to derive radiative parameters like radiative transition probability (A_{rad}), branching ratio (β_r), radiative life time of excited state (τ_r) and stimulated cross-section (σ) etc. and these parameters are presented in Table 4. It has already been noted that the conversion of BO_3 units to BO_4 units takes place with the increase of Bi_2O_3 content, so it seems that the existence of BO_4 units is more suitable for fluorescence. The phonon energy for BO_4 units is less than the corresponding value for BO_3 units and this might be the reason for the enhanced fluorescence as the reduced phonon frequency decreases the rate of non-radiative relaxation.

Therefore high spontaneous emission probability, large branching ratio and low maximum phonon energy is a necessary condition for obtaining fluorescence emission because the emission efficiencies for a rare-earth ion are strongly related to the non-radiative losses from relative excited states. Table 4 shows that the predicted spontaneous emission probability for the transition $^3P_0 \rightarrow {}^3F_2$ increases from 14,347 to 14,607 s^{-1} with increase in Bi_2O_3 concentration. The branching ratio (β_r) is evaluated for each transition and values are presented in Table 4. This table shows that the branching ratio (~42%) for this emission is much larger than other transitions, so this transition ($^3P_0 \rightarrow {}^3F_2$) of Pr^{3+} ions is reasonably efficient in the present host. Fig. 4 depicts the probable lasing transition for the Pr^{3+} ions.

For laser applications, the values of the emission cross-section are of great interest. For calculating the stimulated emission cross-section, first the effective band width, $\Delta\lambda$ has been calculated using

Table 5
Observed IR transmission bands in Pr^{3+} doped zinc bismuth borate glasses.

Sample no.	IR transmission bands (cm^{-1})			
ZBP1	1370	970	670	510
ZBP2	1360	960	680	490
ZBP3	1340	945	675	520
ZBP4	1320	940	680	500
ZBP5	1305	925	685	480

Table 6
Vibration types of different IR wave numbers.

Range of wave numbers (cm^{-1})	Vibration types
420–520	Bi–O–Bi vibration of [BiO_6] octahedral [44,45]
680–720	Bending vibration of B–O–B in [BO_3] triangles [47,48]
900–950	Stretching vibration of [BO_4] units [49]
1200–1300	Stretching vibration of B–O–B in [BO_3] triangles [47,48]

the formula [37]:

$$\Delta\lambda = \frac{\int I(\lambda)d\lambda}{I(\lambda_0)} \quad (11)$$

where $\int I(\lambda)d\lambda$ represents the effective area of the peak and $I(\lambda_0)$ is the intensity of the peak at λ_0. The stimulated emission cross-section has been calculated using Eq. (9) and are listed in Table 4. It is observed that σ increases with increase in Bi_2O_3 content. Therefore, the large stimulated emission cross-section in the present glass is an attractive feature for low-threshold, high gain applications and can be utilized to obtain continuous wave (*CW*) laser action. It has been reported that in Nd^{3+} doped tellurite [38] and lead borate glasses [39], Sm^{3+} doped zinc bismuth borate [35], oxyfluoro-borate [40] and lead fluoro-borate glasses [41], the radiative transition probabilities and the stimulated emission cross-section are large. Laser action has been observed in lead fluoro-borate as well as in tellurite glass systems. Radiative transition probabilities in the present glasses follow the same variations with heavy metal oxides as those reported in zinc bismuth borate [35], lead fluoro-borate [39] and tellurite glasses [38]; therefore the present Pr^{3+} doped zinc bismuth borate glasses may be utilized as potential laser material. Also the values of A_{rad} obtained in the present study are of the same order as reported by Zhang et al. [42] in Pr^{3+} ion doped LKBBT and LKBBG glasses and by Okr et al. [43] in Pr^{3+} ion doped borovanadate glasses.

4.3. Infrared spectroscopy

The IR spectra of the prepared glasses are shown in Fig. 5. From the figure it is observed that the intensity of the band around 510 cm^{-1}, corresponding to Bi–O–Bi vibration of distorted [BiO_6] octahedral units [44,45] increases and the band shifts to lower wave numbers with increase in Bi_2O_3 content (Tables 5 and 6). The absence of the vibration band around 840 cm^{-1} corresponding to [BiO_3] polyhedra [46] implies that only [BiO_6] octahedral units build up the bismuthate structure of the investigated glasses.

The band corresponding to the bending vibration of B–O–B in [BO_3] units shifts from 670 cm^{-1} (ZBP1) to 685 cm^{-1} (ZBP5) [47,48]. This shift may be due to the influence of the electrostatic field associated with the strongly polarizing Bi^{3+} ions. The increase in Bi_2O_3 content results in the increase of the electron cloud density around oxygen of [BO_3] units, thereby, leading to an increase in the roll torque of B–O–B bond and consequently contributes to the shifting of the bending vibration B–O–B bond towards higher wave number. The infrared spectral range 900–950 cm^{-1} (Table 6) is typical for the stretching vibration of [BO_4] units [49]. The existence of [BO_4] units indicates that the addition of Bi_2O_3 into the glass replacing B_2O_3 causes a progressive conversion of [BO_3] units to [BO_4] units. The band between 1200 and 1400 cm^{-1} (Table 6) is assigned to the stretching vibration of [BO_3] units [47,48].

5. Conclusions

The optical properties of Pr^{3+} ions doped zinc bismuth borate glasses have been studied. Effect of bismuth oxide on the absorption and emission spectra were investigated with the help of

Judd–Ofelt theory. The variation of Judd–Ofelt intensity parameters are discussed and correlated to the structural changes in the glass network. Fluorescence intensity is enhanced with the addition of bismuth oxide. Out of three Judd–Ofelt parameters (Ω_λ), the values of Ω_2, which is related to the structural changes in the vicinity of the rare earth ion, indicated covalent environment in zinc bismuth borate glasses. The radiative properties like spontaneous emission probability, radiative life time, branching ratio and stimulated emission cross-section in the present glasses has been determined. The branching ratio for $^3P_0 \rightarrow {}^3F_2$ transition in the present glass is 42% and the predicted spontaneous radiative transition rate is as high as 14,607 s^{-1} for ZBP5 sample. This is beneficial for achieving laser action in Pr^{3+} doped zinc bismuth borate glasses. Further, the radiative emission probability for Pr^{3+} ions these glasses is as high as in lead fluoro- borate glasses, which have been successfully used as laser material. This indicates that the present Pr^{3+} doped zinc bismuth borate glasses can act as potential laser material.

Acknowledgement

Authors are thankful to DST (FIST Scheme) and CSIR, New Delhi, for providing financial support.

References

[1] R. Moorty, M. Jagasin, Mater. Chem. Phys. 93 (2005) 455.
[2] Y.K. Sharma, S.P. Tondon, S.S.L. Surana, Mater. Sci. Eng. B 77 (2000) 167.
[3] Y.C. Ratnakaram, A.V. Kumar, D.T. Naidu, N.O. Gopal, Mater. Lett. 58 (2004) 3908.
[4] K. Wei, D.P. Machewirth, J. Wenzel, E. Snitzer, G.H. Sigel Jr., J. Non-Cryst. Solids 182 (1995) 257.
[5] F. Varsanyi, Appl. Phys. Lett. 19 (1971) 169.
[6] M. Szymanski, J. Karolczak, F. Kaczmarck, J. Appl. Phys. 19 (1975) 345.
[7] J. Hegarty, D.L. Huber, W.M. Yen, Phys. Rev. B 25 (1982) 5638.
[8] S.Q. Man, E.Y.B. Pun, P.S. Cheng, J. Opt. Soc. Am. B 17 (2003) 23.
[9] V.V.R.K. Kumar, A.K. Bhatnagar, R. Jagannathan, J. Phys. D 34 (2001) 1563.
[10] P. Babu, C.K. Jayasankar, Physica B 301 (2001) 326.
[11] K.K. Mahato, D.K. Rai, S.B. Rai, Phys. Stat. Sol. 174 (1999) 277.
[12] W.H. Dumbaugh, J.C. Lapp, J. Am. Ceram. Soc. 75 (1992) 2315.
[13] Z. Pan, S.H. Morgan, K. Dyer, A. Ueda, H. Liu, J. Appl. Phys. 79 (1996) 8906.
[14] S. Tanabe, X. Feng, T. Hanada, Opt. Lett. 25 (2000) 817.
[15] B.R. Judd, Phys. Rev. 127 (1962) 750.
[16] G.S. Ofelt, J. Chem. Phys. 37 (1962) 46.
[17] C.K. Jorgensen, Absorption Spectra and Chemical Bonding in Complexes, Pergamon Press, Oxford, 1962.
[18] R.D. Peacock, The Intensities of lanthanide f–f transitions in: structure and bonding, 22, Springer, Berlin, 1975.
[19] B.R. Judd, Proc. Phys. Soc. London A 69 (1956) 157.
[20] M.J. Weber, D.C. Ziegler, C.A. Angell, J. Appl. Phys. 53 (1982) 4344.
[21] W.T. Carnall, P.R. Fields, K. Rajnak, J. Chem. Phys. 49 (1968) 4443.
[22] C.W. Neilson, G. Fokoster, Spectroscopic Coefficients for the p, d and f configurations, MIT Press, Combridge, MA, 1964.
[23] D.C. Brown, High Peak Power Nd: Glass Laser Systems, Springer, Berlin, 1981.
[24] C.K. Jorgensen, B.R. Judd, Mol. Phys. 8 (1964) 281.
[25] S. Tanabe, T. Ohyagi, N. Soga, T. Hanada, Phys. Rev. B 46 (1992) 3305.
[26] R.D. Peacock, Struct. Bond. 22 (1975) 83.
[27] A. Florez, O.L. Matta, Y. Messaddeq, M.A. Aegereter, J. Non-Cryst. Solids (1997) 213–315.
[28] K. Binnemans, D. Verboven, C.G. Walrand, J. Lucas, N.D. Henary, J.L. Adam, J. Alloys Compd. 250 (1997) 321.
[29] M. Eyal, E. Grennberg, R. Reisfeld, Chem. Phys. Lett. 117 (1985) 108.
[30] P. Nachimuthu, R. Jagannathan, Phys. Chem. Glasses 36 (1995) 77.
[31] R.T. Genova, I.R. Martin, U.R.R. Mendoza, F. Lahoz, A.D.L. Garrin, P. Nunez, J.G. Platas, V. Lavin, J. Alloys Compd. 380 (2004) 167.
[32] L.R. Moorthy, M. Jayasimhadri, A. Radhapathy, R.V.S.S.N. Ravikumar, Mater. Chem. Phys. 93 (2005) 455.
[33] M.A. Newhouse, R.F. Bartholomew, B.G. Aitken, L.J. Button, N.F. Borrelli, IEEE Photonic. Technol. Lett. 6 (1994) 189.
[34] R.S. Quimby, P.A. Tick, N.F. Borrelli, L.K. Cornelius, J. Appl. Phys. 83 (1998) 1649.
[35] A. Agarwal, I. Pal, S. Sanghi, M.P. Aggarwal, Opt. Mater. 32 (2009) 339.
[36] G.H. Dieke, Spectra and Energy Levels of Rare Earth Ions in Crystal, Interscience, New York, 1968.
[37] W. Kochner, Solid-State Laser Engineering, Springer, Berlin, 1996.
[38] M.J. Weber, J.D. Myers, D.H. Biackburn, J. Appl. Phys. 52 (1981) 2944.
[39] M.B. Saisudha, J. Ramakrishna, Phys. Rev. B 53 (1996) 6186.
[40] K.K. Mahato, D.K. Rai, S.B. Rai, Solid State Commun. 108 (1998) 671.
[41] A.G.S. Filho, J.M. Filho, F.E.A. Melo, M.C.C. Custodio, R. Lebullenger, A.C. Hernandes, J. Phys. Chem. Solids 61 (2000) 1535.
[42] Y.Y. Zhang, B.J. Chen, E.Y.B. Pun, H. Lin, Physica B 404 (2009) 1132.
[43] M. El Okr, M. Farouk, M. El-Sherbiny, M.A.K. El-Fayoumi, M.G. Brik, J. Alloys Compd. 490 (2010) 184.
[44] Y. Dimitriev, M. Mihailova, Proceedings of the 16th International Congress on Glass, Vol. 3, Madrid, 1992, p. 293.
[45] M.E. Lines, A.E. Miller, K. Nassau, K.B. Lyons, J. Non-Cryst. Solids 89 (1987) 163.
[46] R. Iordanova, V. Dimitrov, Y. Dimitriev, D. Klissurski, J. Non-Cryst. Solids 180 (1994) 58.
[47] E.I. Kamitsos, A.P. Patsis, M.A. Karakassides, G.D. Chryssikas, J. Non-Cryst. Solids 126 (1990) 52.
[48] A.K. Hassan, L. Borjesson, L.M. Torell, J. Non-Cryst. Solids 172 (1994) 154.
[49] G. El-Damrawi, K. El-Egili, Physica B 299 (2001) 180.